HHS Public Access

Author manuscript

Connectomics Neuroimaging (2017). Author manuscript; available in PMC 2018 June 25.

Published in final edited form as:

Connectomics Neuroimaging (2017). 2017 September ; 10511: 125–133. doi: 10.1007/978-3-319-67159-8_15.

Measuring Brain Connectivity via Shape Analysis of fMRI Time Courses and Spectra

David S. Lee, **Amber Leaver**, **Katherine L. Narr**, **Roger P. Woods**, and **Shantanu H. Joshi**

Ahmanson-Lovelace Brain Mapping Center, Department of Neurology University of California Los Angeles, CA

Abstract

We present a shape matching approach for functional magnetic resonance imaging (fMRI) time course and spectral alignment. We use ideas from differential geometry and functional data analysis to define a functional representation for fMRI signals. The space of fMRI functions is then equipped with a reparameterization invariant Riemannian metric that enables elastic alignment of both amplitude and phase of the fMRI time courses as well as their power spectral densities. Experimental results show significant increases in pairwise node to node correlations and coherences following alignment. We apply this method for finding group differences in connectivity between patients with major depression and healthy controls.

1 Introduction

Patterns of activation in the brain arising from task-based or resting state function magnetic resonance imaging (rfMRI) acquisitions are actively being investigated as potential biomarkers for pathology and healthy development of the brain. Often, network structures in the brain are defined using correlations in spontaneous low-frequency activity from BOLD fMRI signal across different brain areas, either targeting a given region's fMRI timecourse [14, 1] or, less frequently, its power spectrum [12]. Implicit in the computation of correlations and coherence is the linear, one-to-one correspondence between the time series or the spectra, both across regions (i.e. for node to node correlations) and across subjects. This zero-lag assumption may not always hold true due to confounding e ects by neuronal processes, synchronicity between different brain states, physiological noise, or even motion across subjects. Conversely, improved estimation of phase lags may also be informative when inferring directionality in network connections using fMRI data or in comparing the spectral content of fMRI timecourses across different brain regions. Recently researchers have proposed several ideas that compute the extremum of the cross-covariance [8] or perform a frequency-phase analysis [3] to discover this lag structure in rfMRI connectivity.

In our work, we adopt a functional data analysis approach to account for both the amplitude (peaks/valleys) changes and phase (time or frequency) delays when inferring brain connectivity. Here, we would like to define functionalrepresentations of time courses or their spectra and use the functional shape information to align or match them across regions of interests or nodes, or across subjects. This *shape* alignment or matching is performed under a Riemannian metric that naturally gives rise to the connectivity measure that takes both the amplitude and phase into account. Specifically, we use the square root velocity function

(SRVF) [5, 4, 10] to perform functional shape registration [11] of fMRI data. The novelty of our work includes two aspects; a new application of the functional data analysis framework to rfMRI signals, and for the first time we perform functional registration of rfMRI time courses and spectra using the non-linear geometry of a function manifold. To our knowledge this has not been done before. To summarize, the contributions of this paper are as follows: i) analysis of fMRI time courses and spectra using a functional data analysis framework, ii) elastic shape matching of fMRI signals that enables the analysis of both amplitude and phase changes in fMRI across regions, and lastly iii) the use of group level connectivity analysis for detecting changes in patterns of fMRI connectivity across populations.

2 fMRI Shape Analysis of Time courses and Spectra

In this section we describe the functional data analysis approach for analyzing fMRI signals and their spectra. Briefly, functional data analysis (FDA) has been widely applied to several problems in both computer vision and statistics [7, 9, 13]. The main idea is to define an object by a functional representation $f: I \rightarrow \mathbb{R}$, where I is the domain of the function. The function f is assumed to be square-integrable and thus is considered as an element of an infinite-dimensional Hilbert space. This Hilbert space naturally allows the $\mathbb{L}^2$ inner product $\langle f_1, f_2 \rangle = \int_I f_1(t) f_2(t) dt$ that also serves as a metric for finding distances between functions. This framework can then be used to perform statistical modeling including regression, prediction and classification.

2.1 Elastic Functional Data Analysis of fMRI signals using SRVFs

fMRI signal representation: Here, we describe the functional representation for fMRI signals in brief. For more details the reader is referred to [11]. For a given fMRI time course signal $f: I \equiv [0, 1] \rightarrow \mathbb{R}$, and its velocity $\dot{f}(t) = \frac{df}{dt}$ and magnitude $| \dot{f}(t) |$, we define its functional representation by the square-root velocity field (SRVF) map q given by,

$$q: [0, 1] \rightarrow \mathbb{R}, \; q(t) = \frac{\dot{f}(t)}{\sqrt{| \dot{f}(t) |}}. \quad (1)$$

For an absolutely continuous f, the SRVF transformation ensures that q is square integrable. The set of SRVFs is then given by $\mathbb{L}^2\left(\left[0, 1\right], \mathbb{R}\right)$, which is a Hilbert space. The original fMRI signal can be recovered by $f(t) = f(0) + \int_0^t q(\tau) \, | \, q(\tau) \, | \, d\tau$. The SRVF mapping is invertible up to a given $f(0)$. We assume $f(0) = 0$ as the initial condition of the fMRI signal at time $t = 0$. It is noted that the domain I is defined as the interval [0, 1] for all signals in the population. We will use the same notation for denoting the frequency domain spectrum of the fMRI signal given by its power spectral density (PSD) estimate. In this case, the notation for time domain t is changed to that of the frequency domain ν. Then using q for the SRVF mapping, we have $q: [0, 1] \rightarrow \mathbb{R}$, $q(\nu) = \frac{\dot{p}(\nu)}{\sqrt{| \dot{p}(\nu) |}}$, where p is the PSD function of f. With a slight abuse of notation, we will denote q for the SRVF mapping of both the fMRI time course and the PSD.

fMRI temporal domain and spectral domain reparameterization: To account for temporal shifts and spectral phase lags, we now define the notion of time and frequency reparameterization. This idea is closely related to the parameterization (speed) of the underlying domain on which the function f or ν is defined. For example, increasing the speed of the parameterization results in local shrinking of the domain, whereas reducing the speed of the parameterization results in local expansion of the parameterization domain. This behavior can be modeled by a warping function $\gamma: I \rightarrow I$, where $\dot{\gamma} > 0, \forall t \in I$; γ being a diffeomorphism. Thus to change the temporal parameterization, one can simply compose f with γ as $f \circ \gamma$. In the SRVF domain, this is given by

$$q \cdot \gamma = \frac{\left(\dot{f} \circ \gamma\right)\dot{\gamma}}{\sqrt{\left|\left(\dot{f} \circ \gamma\right)\dot{\gamma}\right|}} = \frac{\left(\dot{f} \circ \gamma\right)}{\sqrt{\left|\left(\dot{f} \circ \gamma\right)\right|}}\sqrt{\dot{\gamma}} = (q \circ \gamma)\sqrt{\dot{\gamma}}. \quad (2)$$

We denote the set of all possible γ functions as Γ and emphasize that incorporating domain warping via γ functions enables elastic shape matching of fMRI functions.

Elastic Riemannian metric for SRVFs of fMRI signals: To compare functions and compute distances between them, we define the notion of a metric on the space of q functions. Before analysis of fMRI signals, one usually standardizes the signal by obtaining a z score of f as given by $\tilde{f} = \frac{f - \bar{f}}{\sigma}$, where $\bar{f}$ is the mean value of f and σ is the standard deviation. One can impose an analogous unit length constraint on the q function by obtaining $\tilde{q} = \frac{q}{\| q \|}$. This unit length transformation forces q to lie on a Hilbert sphere denoted by $\mathcal{Q}$. Formally, the space $\mathcal{Q}$ is defined as $\mathcal{Q} \equiv \left\{ q \in \mathbb{L}^2 \mid \int_0^1 \left\langle q(s), q(s) \right\rangle_{\mathbb{R}^2} ds = 1, q(s): [0,1] \rightarrow \mathbb{R}^2 \right\}$. Then one can define the Riemannian metric on the tangent space of this sphere $T_q(\mathcal{Q})$. An important feature of the SRVF representation for fMRI signals is that an elastic Riemannian metric, which is invariant to the domain reparameterization, is reduced to the $\mathbb{L}^2$ metric [11] and given by $d(f_1, f_2) = \| q_1 - q_2 \|$. Therefore, for any two SRVFs given by $q_1, q_2 \in \mathbb{L}^2$ and $\gamma \in \Gamma$, we have $\| q_1 \cdot \gamma - q_2 \cdot \gamma \| = \| q_1 - q_2 \|$. This property allows us to solve the problem of registration in an efficient manner.

2.2 fMRI Alignment and Registration:

Next, we enable comparisons between functions via elastic geodesics between them. Since the space $\mathcal{Q}$ is a Hilbert sphere, the geodesic between two points (shapes) q_1 and q_2 can be expressed analytically as,

$$\chi_t(q_1; v) = \cos\left(t \cos^{-1}\langle q_1, q_2 \rangle\right) q_1 + \sin\left(t \cos^{-1}\langle q_1, q_2 \rangle\right) v, \quad (3)$$

where $t \in [0, 1]$ and the initial tangent vector $v \in T_{q_1}(\mathcal{Q})$ is given by $v = q_2 - \langle q_1, q_2 \rangle q_1$. Then the geodesic distance between the two shapes q_1 and q_2 in $\mathcal{Q}$ is given by

$$d(q_1, q_2) = \int_0^1 \sqrt{\langle \dot{\chi}_t, \dot{\chi}_t \rangle} dt \,. \quad (4)$$

To find the elastic geodesic distance, we simply minimize Eqn. 4 as $d_{\text{elastic}}(q_1, q_2) = \min_{\gamma \in \Gamma} d(q_1, q_2 \cdot \gamma)$. In estimating the elastic geodesic, the optimal reparameterization $\hat{\gamma}$ can be efficiently found as the minimizer $\hat{\gamma} = \text{argmin}_{\gamma}\left(\int_0^1 \| q_1 - \gamma \cdot q_2 \|^2 dt\right)$. In practice, we use dynamic programming to find the optimal $\hat{\gamma}$. The phase difference between two functions is encoded by the warping function $\hat{\gamma}$ resulting from the alignment.

Group analysis and statistics of fMRI signals—For statistical analysis of fMRI signals and spectra, we introduce the notion of the Karcher mean [6]. Given a collection of functions $f_1, f_2, \cdots, f_n$, let $q_1, q_2, \cdots, q_n$ denote their SRVFs, respectively. The Karcher mean is then computed by an iterative procedure: initialize the mean function μ^k at an iteration k and solve for

$$\hat{\gamma}_i^{k+1} = \arg \inf_{\gamma \in \Gamma} \| \mu^k - (q_i \circ \gamma)\sqrt{\dot{\gamma}} \| \,, i = 1, 2, \cdots, n, \quad (5)$$

$$\mu^k = \frac{1}{n} \sum_{i=1}^{n} (q_i \circ \hat{\gamma}_i^{k-1}) \sqrt{\dot{\hat{\gamma}}_i^{k-1}} \,. \quad (6)$$

One can use this mean function as a template for aligning all the functions in the group. This enables one to compare fMRI signals across population.

3 Results

In this section we describe experimental results that show improvement in pairwise node-to-node correlation and coherence as well as group differences in connectivity between healthy controls and patients with major depressive disorder (MDD). 70 patients (34M/36F, mean age 43 years) with MDD and 36 healthy volunteers (17M/19F, mean age 39 years) underwent fMRI imaging on a 3T Siemens Allegra scanner (TR = 2s, TE = 30ms, flip angle = 70, $3.4 \times 3.4 \times 5\ mm^3$ resolution). We used FSL [4] to perform slice-timing correction, motion correction, and high pass filtering. The fMRI scans were then filtered using ICA based denoising and registered to the T1-weighted anatomical MPRAGE scan. All images were normalized to the MNI standard space using SPM [1]. We parcellated the fMRI images using the Craddock functional atlas [2] and focused our analysis on 18 seed regions chosen based on their relevance to depression. They included the subgenual, rostral, and dorsal anterior cingulate cortex (ACC), bilateral amygdala and overlapping anterior hippocampus

(amhp), bilateral dorsolateral prefrontal cortex (DLPFC), bilateral thalamus (Th), posterior cingulate cortex (PCin), and bilateral precuneus (PreCun). Additional regions less relevant to depression were chosen as control nodes; these included bilateral primary visual cortex along the calcarine sulcus (Visual 1 & 2).

3.1 Visualization of Elastic Functional Alignment

Figure 1 shows examples of time course and spectral alignment of fMRI signals across regions and within-subject. In Figure 1, left, non-elastic (Panels A, C, and E γ = identity = t) and elastic matching (Panels B, D, and F) of two time courses and PSDs are compared. In non-elastic matching (Panel A), the two curves are analyzed at each time or frequency, as represented by the vertical black lines. In contrast, in elastic matching (Panel B), similar features of the two curves are aligned. As a result, the peaks and valleys of the two time series in panel F are aligned after elastic matching.

Alignment across subjects allows estimation of a template, which can serve as a reference for group analyses. Figure 2 shows the mean PSDs of the population (N = 106) in 18 regions of interest without and with alignment. While the non-elastic mean seems to capture a single low-frequency feature, the elastic mean identifies features across the frequency range. Finally, Figure 3 shows PSDs of the dorsal anterior cingulate and dorsolateral prefrontal cortex aligned to the average PSD for those ROIs for N = 50 randomly selected subjects. Elastic alignment yields spectra with distinct peaks at both low and high frequencies, mirroring the mean spectra displayed in Figure 3.

3.2 Measuring Brain Connectivity after Elastic fMRI Alignment

Pairwise node to node connectivity measures were obtained by computing the Pearson correlation between time series, coherence between power spectra, and elastic geodesic distances between time series. We remind the reader that the elastic geodesic distance measures the difference between the fMRI signals, whereas measures such as correlation and coherence measure the closeness or agreement between the fMRI signals.

Increases in measures of Correlation and Coherence—As expected we observed increases in correlation and coherence after elastic functional alignment. The effect of alignment was evaluated by comparing correlations of time series and coherences of the PSDs for each pair of nodes across all subjects with and without alignment. Figure 4 shows a signed value of Cohen's d computed as $d(x, x_{aligned}) = \frac{\mu_x - \mu_{x_{aligned}}}{\sigma_{x, x_{aligned}}}$ at each node, where x and $x_{aligned}$ represent the correlations or coherence before and after alignment, respectively. The measures were found to be consistently higher (statistically significant) in majority of connections following alignment. Connectivity among visual cortex was high prior to alignment; therefore changes in these connections were modest.

Population analysis of Connectivity Patterns—Lastly, group differences in functional connectivity between patients and controls were examined using a linear model covaried with age and gender. In addition to the widely used correlation and coherence, we

also used the geodesic distances between nodes and the deviation of the warping function γ from the *identity* as potential measures of connectivity. Figure 5 shows connectivity differences between patients with MDD and healthy controls. Several features in group analysis were observed with alignment. Some connections represented by correlation or coherence were maintained with alignment, for example, between anterior cingulate and dorsal prefrontal cortex. Importantly, effect sizes of the group differences increased for existing connections after alignment. Not all connections were preserved after alignment. For example, the correlations between the precuneus and thalamus were weakened after alignment. On the other hand, the correlation and coherence between posterior cingulate and thalamus were increased after alignment.

4 Discussion

We proposed an elastic shape matching approach for the analysis of fMRI time series and PSDs. It is worth noting that several significant inter-node connections shown by elastic geodesic and gamma distances coincided with those shown by correlation or coherence. For example, significantly higher correlation after alignment, and coherence before and after alignment between thalamus and medial anterior cingulate are captured by lower geodesic and gamma distances. On the other hand, the lower correlation in controls between precuneus and thalamus is encoded by a higher gamma distance, whereas lower coherence in controls between posterior cingulate and thalamus is encoded by higher geodesic distances. This suggests that the geodesic and gamma distances from elastic alignment may serve as additional representation of connectivity. While we observed increase in correlation and coherence between fMRI signals following alignment, further validation will be necessary to explore the clinical utility of this approach. In addition, we anticipate enhanced effect of alignment in task-based fMRI where neurobiological signals are coherent with tasks.

Acknowledgments

This research was supported by the NIH/NIAAA award K25AA024192, and the NIH/NIMH awards K24MH102743 and U01MH110008.

References

1. Baria AT, Baliki MN, Parrish T, and Apkarian AV. Anatomical and functional assemblies of brain bold oscillations. Journal of Neuroscience, 31(21):7910–7919, 2011. [PubMed: 21613505]
2. Craddock RC, James GA, Holtzheimer PE, Hu XP, and Mayberg HS. A whole brain fMRI atlas generated via spatially constrained spectral clustering. Human brain mapping, 33(8):1914–1928, 2012. [PubMed: 21769991]
3. Goelman G, Dan R, Růžička F, Bezdicek O, Růžička E, Roth J, Vymazal J, and Jech R. Frequency-phase analysis of resting-state functional MRI. Scientific Reports, 7, 2017.
4. Joshi SH, Klassen E, Srivastava A, and Jermyn I. A novel representation for Riemannian analysis of elastic curves in R^n. In IEEE Conference on Computer Vision and Pattern Recognition (CVPR), pages 1–7. IEEE, 2007.
5. Joshi SH, Klassen E, Srivastava A, and Jermyn I. Removing shape-preserving transformations in square-root elastic (SRE) framework for shape analysis of curves In Energy Minimization Methods in Computer Vision and Pattern Recognition (EMMCVPR), pages 387–398, 2007.
6. Karcher H. Riemannian center of mass and mollifier smoothing. Communications on Pure and Applied Mathematics, 30:509–541, 1977.

7. Kneip A and Ramsay JO. Combining registration and fitting for functional models. Journal of the American Statistical Association, 103(483):1155–1165, 2008.
8. Mitra A, Snyder AZ, Hacker CD, and Raichle ME. Lag structure in resting-state fMRI. Journal of neurophysiology, 111(11):2374–2391, 2014. [PubMed: 24598530]
9. Ramsay JO and Li X. Curve registration. Journal of the Royal Statistical Society: Series B (Statistical Methodology), 60(2):351–363, 1998.
10. Srivastava A, Klassen E, Joshi SH, and Jermyn IH. Shape analysis of elastic curves in Euclidean spaces. IEEE Trans. on Pattern Analysis and Machine Intelligence, 33:1415–1428, 2011.
11. Srivastava A, Wu W, Kurtek S, Klassen E, and Marron JS. Registration of functional data using Fisher-Rao metric. arXiv:1103.3817v2, 2011.
12. Sun FT, Miller LM, and D'Esposito M. Measuring interregional functional connectivity using coherence and partial coherence analyses of fMRI data. Neuroimage, 21(2):647–658, 2004. [PubMed: 14980567]
13. Tang R and Muller H-G. Pairwise curve synchronization for functional data. Biometrika, 95(4): 875–889, 2008.
14. Zuo X-N, Di Martino A, Kelly C, Shehzad ZE, Gee DG, Klein DF, Castellanos FX, Biswal BB, and Milham MP. The oscillating brain: complex and reliable. Neuroimage, 49(2):1432–1445, 2010. [PubMed: 19782143]

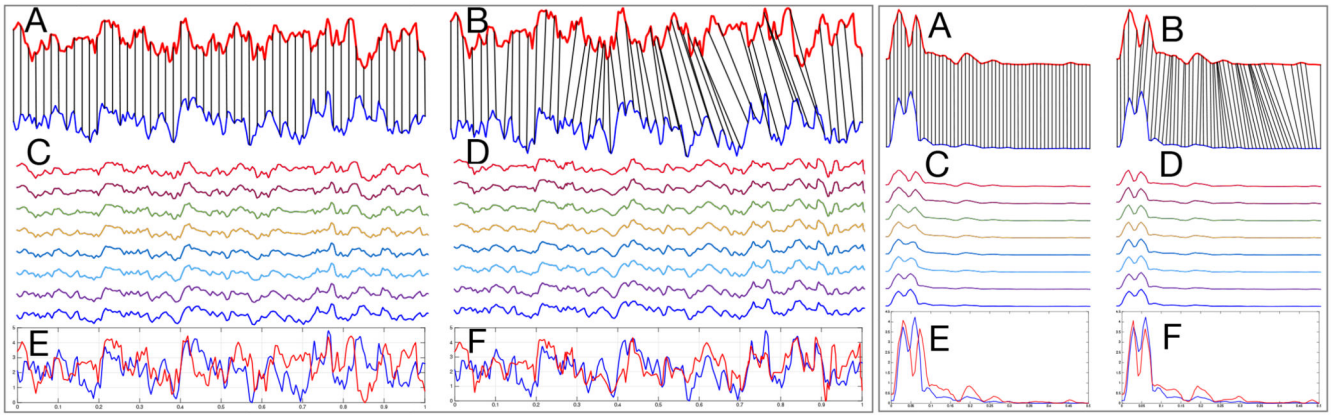

Fig. 1.

Within-subject registration of resting state time courses (Left), and power spectral densities (PSDs, Right). A: non-elastic matching between the top and bottom fMRI signals. B: elastic matching shown by corresponding lines. C: non-elastic and D: elastic geodesics between the two time signals (Left), or PSDs (Right). E: overlay of top and bottom signals before matching. F: overlay after matching.

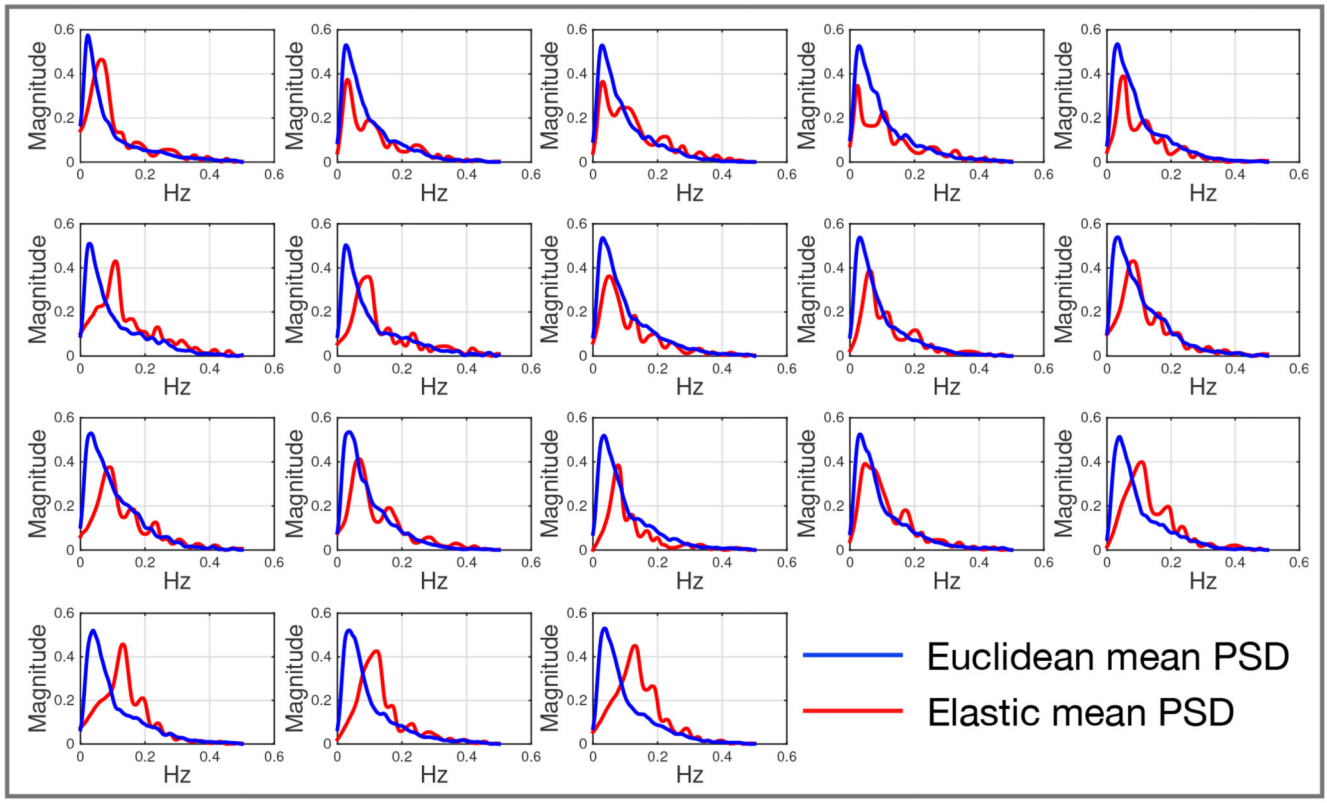

Fig. 2.
Mean PSDs for 18 regions of interest.

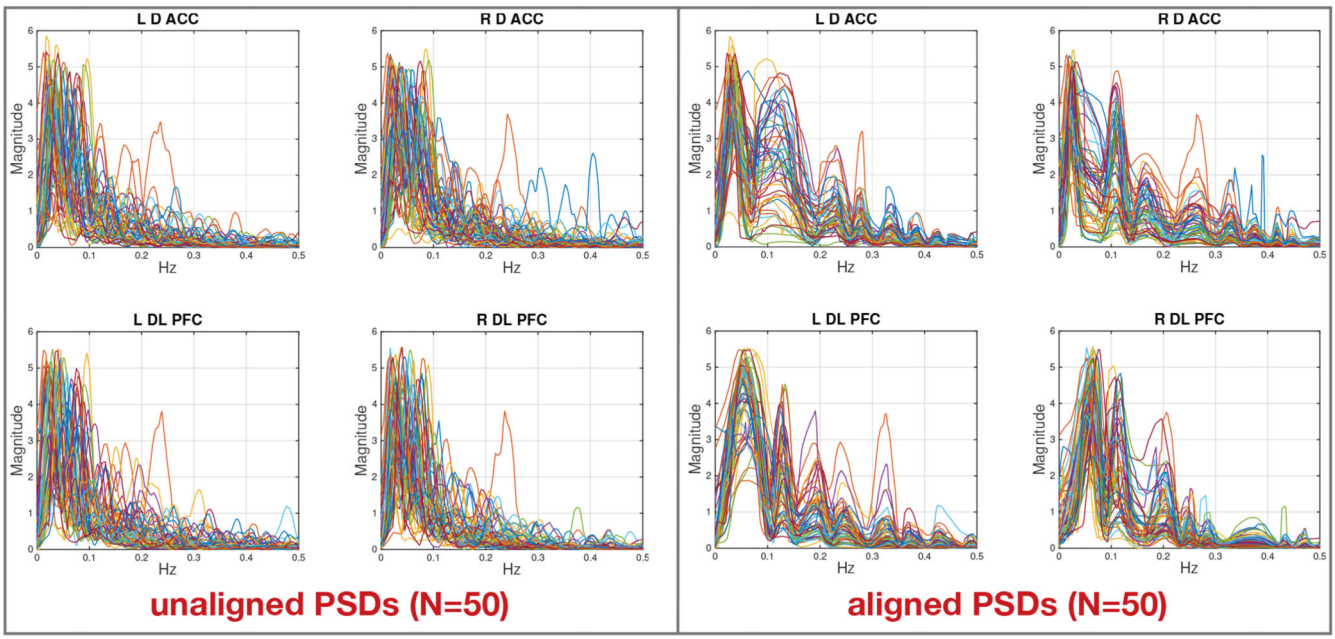

Fig. 3.

Left panel: Unaligned PSDs overlaid; each line corresponds to data from a single subject. Right panel: PSDs after elastic alignment to the mean shape. ROIs shown are the left and right dorsal anterior cingulate and the left and right prefrontal cortex.

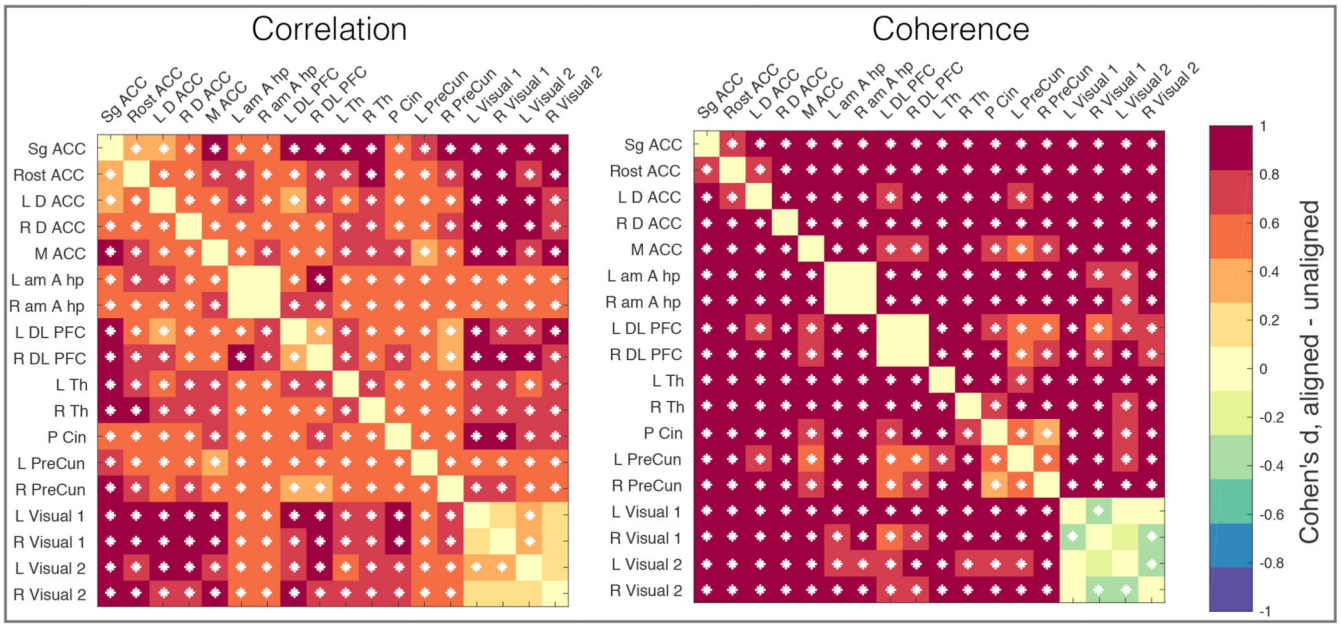

Fig. 4.

Signed Cohen's d shown at each node, with a white asterisk denoting significance at $p < 0.05$ (uncorrected). ACC-Anterior Cingulate Cortex; Am A hp-Amygdala/Anterior hippocampus; Cin-Cingulate; D-Dorsal; L-Left; P-Posterior; PreCun-Precuneus; R-Right; Rost-Rostral; Sg-Subgenual.

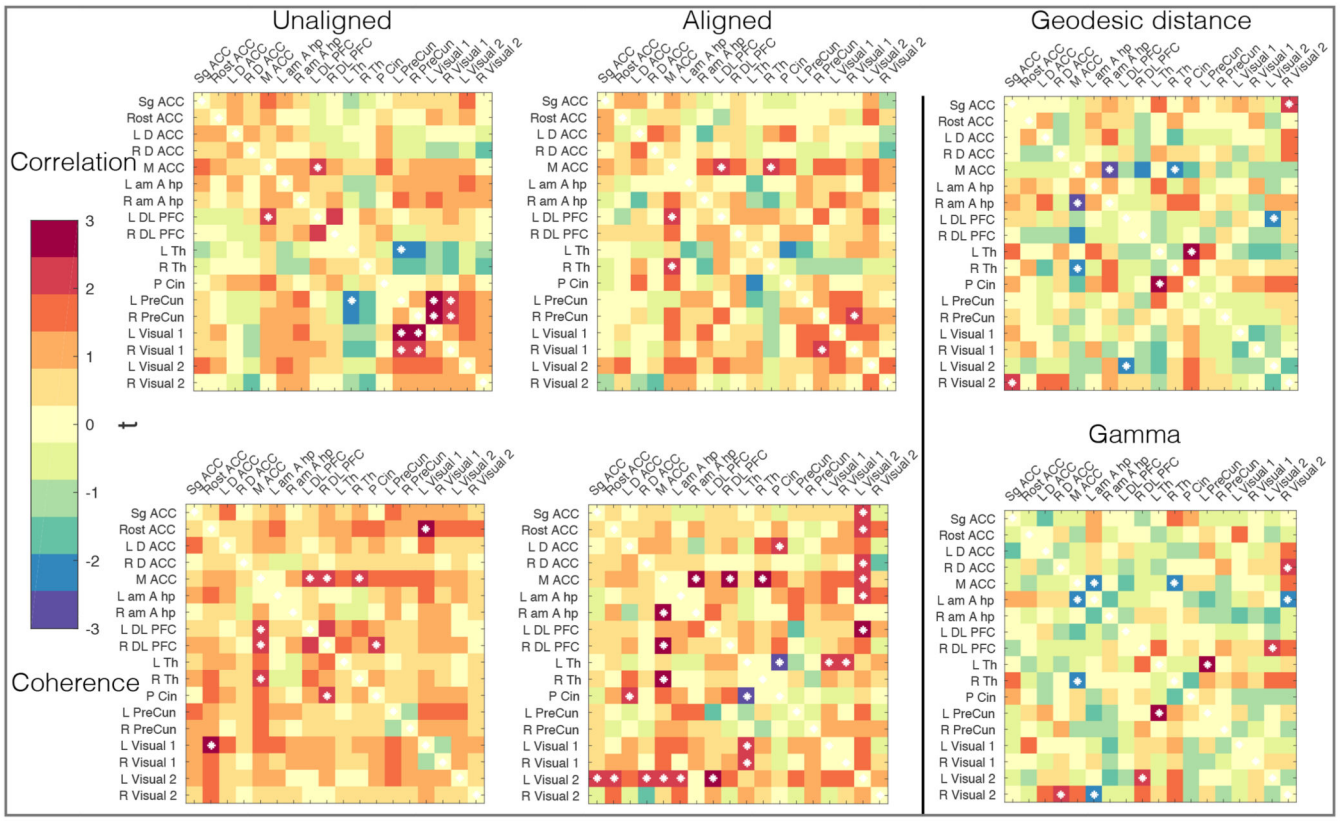

Fig. 5.

Group (differences between patients with MDD and healthy controls. Colormap shows the t-statistic with controls > patients. The white asterisk denotes pairwise significance at $p < 0.05$ (uncorrected).